The Photo-Injected Fresnel Zone Plate Antenna: Optoelectronic Beam Steering at mm-Wave Frequencies

Tom F. Gallacher, *Student Member, IEEE*, Duncan A. Robertson, *Member, IEEE*, and Graham M. Smith

***Abstract*—We present an overview of the photo-injected Fresnel zone plate antenna (piFZPA) method for non-mechanical optoelectronic beam steering. The piFZPA method enables rapid beam steering, over moderate field-of-views, at both mm-wave and submm-wave frequencies, that is suitable for a wide range of imaging and non-imaging applications. This paper develops a theoretical framework that details the design of piFZPAs and provides an understanding to, and optimization of, the piFZPA performance. As an example device, we present preliminary experimental scanning data on a transmission-type piFZPA, operating at 94 GHz, that relies on commercially available visible display technologies for plasma generation and reconfiguration. The experimental data is shown to agree well with numerical simulations and validates the theoretical framework.**

***Index Terms*—Beam forming, beam steering, Fresnel zone plate, optically controlled antenna, optoelectronic, photo-injected Fresnel zone plate.**

I. Introduction

MANY mm-wave and submm-wave applications, such as imaging, surveillance and remote sensing, demand rapid beam steering capabilities in order to meet their technological goals. However, the continued high cost of receivers at these frequencies often result in implementations based on a limited number of detectors (or just one) in conjunction with a beam steering mechanism. While much research has been focused on suitable beam steering technologies, such as phased arrays, reflectarrays, and Rotman lenses, these solutions often suffer from a number of disadvantages such as: limited reconfigurability, 1-D scanning, complex architectures, high component counts, high losses, and/or high costs. These technologies can also prove difficult to realize at higher submm-wave frequencies.

Manuscript received April 20, 2012; revised November 28, 2012; accepted December 16, 2012. Date of publication January 04, 2013; date of current version April 03, 2013. This work was supported by the U.K. Engineering And Physical Sciences Research Council (EPSRC).

T. F. Gallacher was with the SUPA, School of Physics and Astronomy, University of St Andrews, St Andrews, Fife KY16 9SS, U.K. He is now with the Department of Radio Science and Engineering, SMARAD/MilliLab, Aalto University School of Electrical Engineering, FI-00076 Aalto, Finland (e-mail: thomas.gallacher@gmail.com).

D. A. Robertson and G. M. Smith are with the SUPA, School of Physics and Astronomy, University of St Andrews, St Andrews, Fife, KY16 9SS, U.K.

Color versions of one or more of the figures in this paper are available online at http://ieeexplore.ieee.org.

Digital Object Identifier 10.1109/TAP.2012.2237004

Comparatively, the use of optically excited semiconductors have been shown to offer promising devices at high frequencies, such as fast RF switches, attenuators, and phase shifters [1], and have the potential for creating non-mechanical scanning devices, such as optically controlled gratings [2], or zone plates. Optically controlled Fresnel zone plates were first demonstrated by G. W. Webb *et al.* [3]–[6] nearly twenty years ago, which featured a bespoke and complex array of individually controlled near infrared (NIR) LEDs. Since this time, few details on the design, requirements and limitations of photo-injected Fresnel zone plates (piFZPAs) at (sub)mm-wave frequencies have been presented. Using optimized silicon wafers, detailed in prior work [7], we present initial experiments which demonstrate practical piFZPAs at 94 GHz using standard *visible* display technologies.

The following discussions aim to provide a theoretical framework which will enable optimized design of piFZPAs at (sub)mm-wave frequencies. While the following demonstrations feature the lower efficient transmission-type piFZPA (see Section III), and are far from optimal, these initial demonstrations provide an insight into the potential impact of this technology. Using optimized visible display technologies and piFZPA design, piFZPAs have the ability to enable highly flexible and arbitrary 3-D non-mechanical scanning and beam forming, which is scalable to high mm- and submm-wave frequencies, larger diameters, and which can provide rapid beam steering over moderate field-of-views, whilst also being simple and of moderate costs. Thus, the piFZPA method is a potentially attractive non-mechanical beam steering solution, suitable for a host of applications.

II. The piFZPA

The photo-injected Fresnel zone plate antenna (piFZPA) encompasses the optical excitation of a Fresnel zone plate plasma within a semiconductor substrate. Optical reconfiguration of the zone plate plasma then permits non-mechanical beam forming and dynamic steering in 1-, 2- or 3-dimensions.

piFZPAs can be realized in one of two configurations: transmission (tx) or reflection (rx) types. Both configurations are limited to half-wave correction schemes [8] due to the limitation imposed by the semiconductor substrate, i.e. optically controlled attenuation. Under this scheme, piFZPAs are inherently limited to a maximum of 40% radiation efficiency (c.f. traditional phase-correcting/reversal Fresnel zone plates [8]). In addition, the required optical power and scan rate of piFZPAs are inversely related via the minority free-carrier effective lifetime

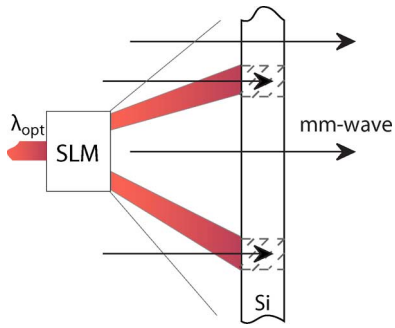

Fig. 1. Depiction of the transmission-type piFZPA, which represents a reconfigurable analogue to a classic (Soret) blocking-type zone plate.

parameter. Thus, faster scanning piFZPAs require more optical power than their slower counterparts. Nevertheless, these disadvantages are often out-weighed by their flexibility, speed, fidelity, system complexity and cost.

The following sections describe each piFZPA configuration, detailing their design, requirements, and optimization.

III. Transmission-Type piFZPAs

The transmission-type piFZPA (tx-piFZPA) is the simplest of the two configurations to realize, and represents a reconfigurable analogue to the classic blocking-type zone plate structure; this design scheme results in a maximum radiation efficiency of 10% [8]—or a 10 dB loss. Although low in efficiency, the diffraction limited performance and flexible beam steering capabilities of tx-piFZPAs maintains their attraction for applications requiring arbitrary, rapid beam steering, and that are not limited by signal-to-noise, such as imaging applications; similar to their classic counterparts.

In its basic form, the transmission-type configuration includes an optical source, optical spatial light modulator (SLM), suitable semiconductor substrate, relevant mm-wave hardware for transmit/receive, and a suitable means of illuminating the substrate by both optical and mm-wave beams, typically by means of an optically transparent mm-wave reflector. Fig. 1 depicts the essence of the transmission-type configuration.

Using Fig. 1, the optical source excites a free-carrier plasma with distinct spatial features which are defined by the zone plate mask, optically encoded by means of the optical SLM. Using suitable means to align both optical and mm-wave beams onto the semiconductor substrate, a mm-wave beam is propagated through the substrate using relevant quasi-optical components. Optical reconfiguration of the zone mask via the SLM then permits dynamic steering of the mm-wave beam using the opto-excited plasma. This enables the realization of a generalized (sub) mm-wave SLM capable of producing adaptive beam forming and non-mechanical beam steering.

A. Design

The design of transmission-type piFZPAs involves calculation of both the zone plate structure and the substrate thickness. The zone plate design defines the overall antenna performance and pointing direction, whilst appropriate substrate thicknesses are required in order to minimise the dark-state insertion loss through the substrate. The zone plate design, or radii, r_n, are calculated using the standard zone plate equation for a half-wave correction scheme [8]:

$$r_n = \sqrt{n\lambda F + \left(\frac{n\lambda}{2}\right)^2}, \tag{1}$$

with a given focal length F, mm-wave design wavelength λ, and zone number, n. Optimal substrate thicknesses are calculated using the standard expression for a matched Fabry-Pérot etalon [9]:

$$d = \frac{m\lambda}{2\sqrt{\epsilon_r'}} \qquad m = 1, 2, 3, \ldots \tag{2}$$

where for the piFZPA, ϵ_r' denotes the substrate dark permittivity, with $\epsilon_r' = 11.7$ for silicon [1].

While the design of the piFZPA follows simply from (1) and (2), practical realization of such devices requires consideration to the spatial resolution of the opto-excited plasma, defined by the ambipolar diffusion length, L_a. As a result, zone plate designs are limited to designs which maintain zone widths greater than L_a [7], [9]. Thus, appropriate F/D designs must be considered in order to ensure good amplitude taper whilst also ensuring sufficiently large zone widths: the performance of piFZPAs become degraded due to non-negligible lateral diffusion (see Section V), for zone plate designs featuring zone widths that are comparable to, or less than, the substrate diffusion length.

B. Plasma Density Requirements

One of the most important parameters of interest in the design and analysis of piFZPAs is the effective free-carrier plasma density, Δn. The transmission-type piFZPA presents alternate regions of low and high absorption which thus represents a reconfigurable analogue to the standard Soret, or blocking, Fresnel zone plate [8], [9]. In order to achieve the maximum radiation efficiency of the reconfigurable blocking zone plate (10%) the optically excited plasma regions must produce metallic-like behavior. However, such high plasma densities ($> 10^{16}$ cm^{-3} for silicon) require large irradiation densities that are often impractical (i.e. high power laser irradiation); nevertheless, much lower plasma densities may be implemented with minimal degradation to the piFZPA efficiency. The piFZPA plasma dependent performance and requirements can be found by using a composite piFZPA model, which has been shown to agree extremely well with experimental data [9].

Fig. 2 displays the simulated far-field antenna patterns for an F/2, 100 mm diameter transmission-type piFZPA with a substrate thickness of $d = 466$ μm, for a range of effective plasma densities, at 94 GHz. It is observed that the formation of a directive mainlobe becomes more evident as the effective plasma density of each alternate zone increases (increased attenuation), with a plasma density creating an attenuation of 6 dB showing to provide acceptable performance including an increase in gain, directivity, and sidelobe suppression. From these simulations, a photo-injected attenuation of 6 dB ($\Delta n = 8.3 \times 10^{14}$ cm^{-3} in

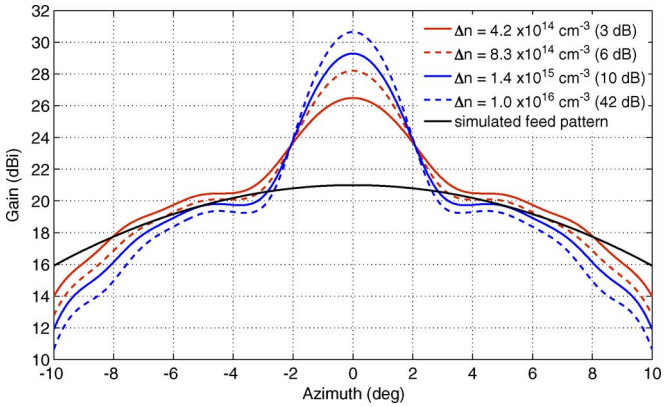

Fig. 2. Simulated far-field patterns for a $d = 466\ \mu\mathrm{m}$ thick substrate, F/2 100 mm aperture piFZPA. Simulations suggest beam formation for optically injected losses exceeding ~6 dB ($\Delta n = 8.3 \times 10^{14}\ \mathrm{cm}^{-3}$), with increased sidelobe suppression and gain for losses exceeding 10 dB.

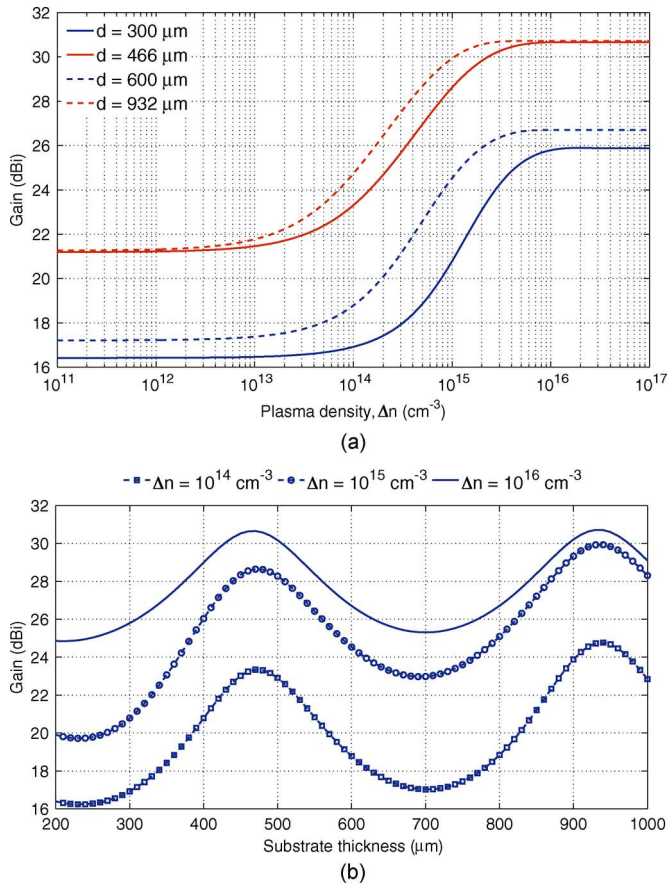

Fig. 3. Simulated gain variation for a F/2, 100 mm diameter transmission-type piFZPA as (a) a function of the effective plasma density Δn, and (b) a function of substrate thickness d.

this case) can be considered to be the minimum required attenuation level for reasonable piFZPA performance, which corresponds to a ~3 dB reduction from the maximum achievable gain (10 dB below the directive gain, from above). This opto-excited state represents a practical compromise between the required irradiation level, the sidelobe suppression, directivity, and overall antenna radiation efficiency ($\eta > 5\%$). Nonetheless, an opto-injected attenuation of 10 dB is shown to offer better performance, for a modest increase in irradiance, with better than 7% radiation efficiency and near diffraction limited performance (neglecting diffusion effects).

The minimal photo-injected attenuation level will depend on the available optical power from the chosen light source and the required antenna performance for the given application. Most importantly, this analysis indicates that a much lower effective plasma density can be tolerated, whilst maintaining reasonable antenna performance. Thus a full optically induced metallic zone plate is not required, albeit resulting in a modest reduction in antenna performance.

C. Optimization

In general, the piFZPA performance will require optimization of both the plasma density, Δn, and the substrate thickness, d; the optimization of the illumination wavelength has been detailed in previous work [7]. Fig. 3 displays the gain variation for a transmission-type piFZPA as a function of the effective plasma density, Δn, for a selection of substrate thicknesses, Fig. 3(a); and also as a function of substrate thickness for a selection of plasma densities, Fig. 3(b). The simulations were performed using the same composite piFZPA model as before, and were for a 100 mm diameter transmission-type piFZPA with a 200 mm focal length. An effective plasma density of $10^{11}\ \mathrm{cm}^{-3}$ corresponds to the background carrier density (high-resistivity silicon sample), which then gives the gain of the simulated feed (approx. 21 dBi).

Considering the optimization of the effective plasma density first, Fig. 3(a) displays the gain as a function of the effective plasma density, Δn, for substrate thicknesses $d = 300$, 466, 600, and 932 μm. Here, $d = 466$ and 932 μm correspond to substrate thicknesses which are resonantly matched at 94 GHz, defined by (2) with $m = 1, 2$ respectively. The relative change in antenna gain, for each substrate thickness, is observed to rise gradually as the effective plasma density increases, which would be expected due to the increased loss through the substrate. The antenna gain is also shown to saturate in all cases beyond a carrier density of $\Delta n = 10^{16}\ \mathrm{cm}^{-3}$, corresponding to alternating opto-excited metallic-like zones, i.e. a classical blocking-type zone plate. Moreover, for resonantly matched substrate thicknesses ($d = 466$, 932 μm), the saturation level is shown to peak at 31 dBi, corresponding to an approximate radiation efficiency of 10%, matching with standard zone plate theory.

Fig. 3(a) also indicates a lower plasma density for the transition period to increased gain when the thickness of the semiconductor substrate is increased, i.e going from $m = 1 \rightarrow m = 2$, which results from the increased attenuation at a given injection level from the increased substrate thickness; noting that a longitudinal homogeneous plasma distribution is assumed for all thicknesses. However, this assumption becomes invalid as the substrate thickness increases, arising from the diffusion limit of the free-carrier plasma, which leads to lowered effective plasma densities. Nevertheless, a homogeneous plasma distribution remains valid for substrates which feature large free-carrier lifetimes, leading to comparable, or greater, diffusion lengths than the substrate thickness. For example, a free-carrier effective lifetime of $\tau_{\mathrm{eff}} \geq 350\ \mu$s (reasonable for moderate quality silicon)

leads to a diffusion length (L_a) of approximately 1 mm, depending on the substrate.

Non-resonantly matched substrates are shown to yield reduced piFZPA gain due to the increased loss through the semiconductor etalon. This gives rise to the lowered gain observed for the $d = 300$, 600 μm cases, and gives rise to the apparent reduced feed gain (<21 dBi).

Considering the substrate thickness further, Fig. 3(b) displays the corresponding gain as a function of substrate thickness, d, with effective plasma densities $\Delta n = 10^{14}$, 10^{15} cm^{-3}, and 10^{16} cm^{-3}. The piFZPA gain is shown to oscillate as a function of substrate thickness, where maximum gain is observed for substrate thicknesses satisfying (2); the oscillations and peak gain correspond to the matching of the transmission-mode semiconductor etalon. Furthermore, the peak gain in the oscillations are shown to be invariant for the $\Delta n = 10^{16}$ cm^{-3} case, whilst higher gain is observed at higher order $(m > 1)$ matched substrate thicknesses for effective plasma densities $\Delta n < 10^{16}$ cm^{-3}. The gain invariance of the $\Delta n = 10^{16}$ cm^{-3} case results from the saturation of the transmission-type piFZPA efficiency, while the higher gain for substrates of increased thickness $(m > 1)$ result from the increased attenuation at the given effective plasma density, where a homogeneous plasma distribution has been assumed.

Thus it is clear that both the substrate thickness and the effective photo-injected plasma density significantly affect the gain of the transmission-type piFZPA, with the maximal case corresponding to resonantly matched substrate thicknesses and with optically excited plasma densities exceeding the metallic limit ($\geq 10^{16}$ cm^{-3}, for silicon). Both parameters yield a maximum 10% radiation efficiency, or 10 dB reduction from the directive gain, D, which scales with the aperture size of the piFZPA.

IV. Reflection-Type piFZPAs

Now we consider the second configuration: the reflection-type piFZPA. The reflection-type piFZPA (rx-piFZPA), while more challenging to realise in practice due to increased substrate thickness dependencies, features two modes of operation: the improved blocking-type piFZPA, and the phase-reversal piFZPA. The former features the same 10% radiation efficiency of the transmission-type piFZPA, but with a lower plasma density requirement, while the latter, which was first identified in US patents [10], [11], yields increased radiation efficiencies of up to 40%, with a corresponding increase in the required plasma density. As a result, the reflection-type piFZPA may present a more attractive option for most applications. Both configurations of the reflection-type piFZPA are depicted in Fig. 4.

The reflection-type piFZPA typically requires an on-axis feed, and thus will suffer from aperture blockage effects. However, such effects can be minimized by appropriate dimensioning of the feed.

The components and operation of the reflection-type piFZPA configuration follow, similarly, the transmission-type piFZPA, but with a requirement of an optically transparent mm-wave reflector due to the illumination configuration. Typical optically transparent mm-wave reflectors include either a fine wired polarizer mesh or grid, or conductive polymer films. In general, conductive polymer films are preferred due to their higher optical transmission and reasonable mm-wave reflectivity.

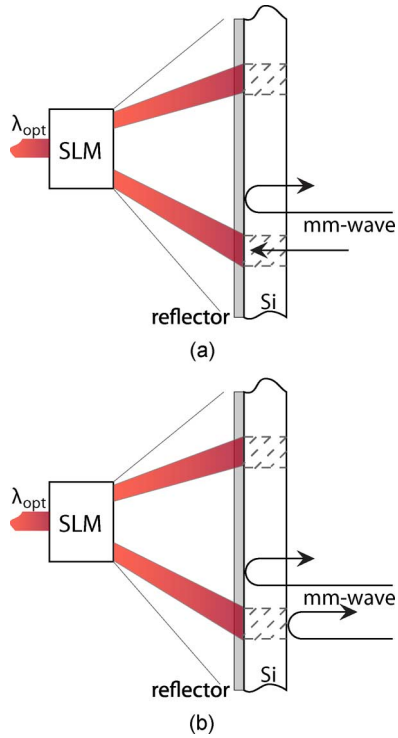

Fig. 4. Depiction of the reflection-type piFZPA illustrating the (a) improved blocking, and (b) the phase-reversal subgroups.

A. Design

The design of reflection-type piFZPAs follows a similar procedure as set by the transmission-type. The zone plate design follows that set above, with the design of each zone plate radii, r_n given by (1); where the substrate thickness requires a match to the reflection mode etalon such that reflection from the semiconductor substrate is maximized. Following the standard expression for a reflection mode etalon, the semiconductor substrate thickness can be calculated using [9]

$$d = \frac{m\lambda}{4\sqrt{\epsilon_r'}} \qquad m = 1, 3, 5, \ldots \tag{3}$$

where each term has been defined above.

Note that the reduced substrate thickness, which results from the reflection-mode etalon, presents an increased sensitivity to surface defects; thus substrate processing or higher order substrate thicknesses $(m > 1)$ are generally required in order to reduce surface mediated losses of optically excited carriers [9].

B. Plasma Density Requirements

The plasma density requirements, and the mode of operation, for the reflection-type piFZPA configuration are best modelled using a standard reflection-mode etalon model [9]. This model, in conjunction with the behavior depicted in Fig. 3, details the reflection-type performance and trends.

Fig. 5 displays the simulated fractional field reflectivity, r', and the corresponding phase change, ϕ, through a reflection-

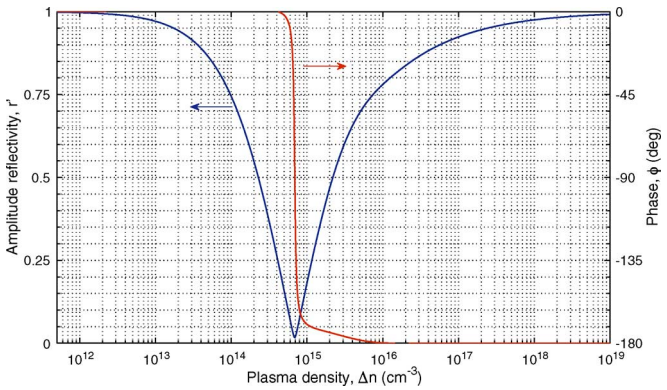

Fig. 5. Simulated reflectivity and phase from a reflection-type piFZPA transmission line. The reflection-type etalon yields increased sensitivity to changes in the complex permittivity leading to minimized reflection at lower carrier densities. A 180° phase change is shown, with near unity reflected amplitude due to an opto-excited metallic state.

type piFZPA transmission line as a function of the photo-injected plasma density, Δn, for a substrate thickness $d = 233\ \mu\mathrm{m}$ [$\mathrm{m} = 1$ in (3)] at 94 GHz. Simulations show that the reflectivity is maximal for a high-resistivity sample ($\Delta n = 10^{11}\ \mathrm{cm}^{-3}$), as would be expected for the chosen substrate thickness. Using this point as a reference (amplitude and phase), the amplitude reflectivity is shown to approach zero as the plasma density increases, reaching a minimum at $\Delta n = 6.9 \times 10^{14}\ \mathrm{cm}^{-3}$, resulting from the increased loss presented by the opto-excited substrate (i.e. etalon becomes unmatched). At this carrier density, the matched etalon thickness gives near-perfect ($r' \sim 0.01$) cancellation of the reflected beam with a near 180° phase change through the transmission line. Fractional adjustment of the substrate thickness may yield further cancellation of the reflected beam, with increased phase change [11].

Using Fig. 5 as an example reflection-type piFZPA design, a blocking reflection-type piFZPA can then be realized for alternating opto-excited zones with an effective plasma density of $\Delta n = 6.9 \times 10^{14}\ \mathrm{cm}^{-3}$, with the un-illuminated zones corresponding to $\Delta n \geq 10^{11}\ \mathrm{cm}^{-3}$ (depending on substrate resistivity). The reflection minimum, which gives 1% (amplitude) reflection in the matched etalon case, shown in Fig. 5, corresponds to a 40 dB contrast between the illuminated and un-illuminated zones. This is equivalent to the maximum radiation efficiency (10%) case of the transmission half-wave blocking correction scheme (Section III). Most importantly, the required effective plasma density is more than an order of magnitude lower for the blocking reflection-type piFZPA than the transmission-type piFZPA ($\Delta n = 6.9 \times 10^{14}\ \mathrm{cm}^{-3}$ vs. $\Delta n \geq 10^{16}\ \mathrm{cm}^{-3}$), due to the increased finesse of the reflection mode etalon; this has been coined '*the improved blocking Fresnel zone plate antenna*' [11]. Degradation of the antenna efficiency from its maximum value, for effective plasma densities located at either side of the minimum point, follow the effective plasma density degradation shown in the transmission-type configuration discussed previously (see Fig. 3).

The second configuration of the reflection-type piFZPA is also evident from Fig. 5. Increased effective plasma densities beyond the reflection minimum ($\Delta n > 6.9 \times 10^{14}\ \mathrm{cm}^{-3}$) result in a continued increase in the amplitude reflectivity, whilst maintaining a constant 180° phase change. The transition towards perfect amplitude reflectivity with a 180° phase change results from the transition to the standard *low-frequency limit*, where the opto-excited zones begin to produce metallic-like behaviour [9].

The phase-reversal piFZPA, depicted in Fig. 4(b), yields a maximum efficiency of 40% due to the half-wave correction zone plate scheme and full use of the incident energy from the feed, c.f. half-wave phase-correcting zone plate [8]. From Fig. 5, perfect amplitude reflectivity and 180° phase change is shown to require an effective plasma density of $\Delta n \approx 10^{19}\ \mathrm{cm}^{-3}$. However, this very large plasma density may be relaxed to plasma densities exceeding $10^{16}\ \mathrm{cm}^{-3}$, which yields greater than 80% amplitude reflectivity. A reflection-type, phase-reversal piFZPA with alternating illuminated zones greater than this density would suffer a modest degradation from the maximum radiation efficiency, with the power reflectivity dropping by less than 2 dB. Thus a higher (radiation) efficiency reflection-type piFZPA can be realized for a similar effective plasma density as that required in the transmission-type piFZPA!

C. Optimization

Optimization of the reflection-type piFZPA configuration is subject to the same limitations which are imposed by the substrate diffusion length discussed above, in addition to control of the effective plasma density and substrate thickness.

Fig. 6(a) indicates both the change in amplitude reflectivity and phase change for slight deviations in the matched substrate thickness, given by (3). The tolerance on substrate thickness deviations has been modelled for a first order ($\mathrm{m} = 1$) substrate thickness at 94 GHz, i.e. $d = 233\ \mu\mathrm{m}$.

From Fig. 6(a), small deviations in substrate thickness are shown to increase the reflection minimum and phase. For example, an attenuation contrast between the reflection minimum and the dark state ($\Delta n \approx 10^{11}\ \mathrm{cm}^{-3}$) changes from 40 dB on resonance to 17 dB for a 5% (12 $\mu\mathrm{m}$) deviation from the matched substrate thickness, reducing to 12 dB for a 10% (24 $\mu\mathrm{m}$) deviation in substrate thickness. Thus, small changes in the substrate thickness from the matched case result in reduced radiation efficiency, similar to the transmission-type, where for example the 5% case would yield an radiation efficiency $7\% \geq \eta \geq 10\%$, c.f. Fig. 3(a). A similar effect (for a resonantly matched thickness) would also be observed if the opto-excited plasma density were to correspond to either side of the reflection minimum. A similar degradation will be expected for the phase-reversal case due to the lowered phase change as a result of the deviation, i.e. $\eta < 40\%$. The sensitivity to the substrate thickness is higher in the reflection-type configuration than in the transmission-type piFZPA due to the increased finesse of the reflection-mode etalon created by the reflector-backed semiconductor substrate [9].

Assuming homogeneous plasma distribution, higher order substrate thicknesses ($m = 3, 5, \ldots$) result in a shift of the reflection minimum to lower effective plasma densities due to the increased loss through the substrate. The shift is observed for both the improved blocking and phase reversal piFZPA configurations, illustrated in Fig. 6(b), which displays the amplitude and phase for the $m = 1$ and $m = 3$ cases at 94 GHz.

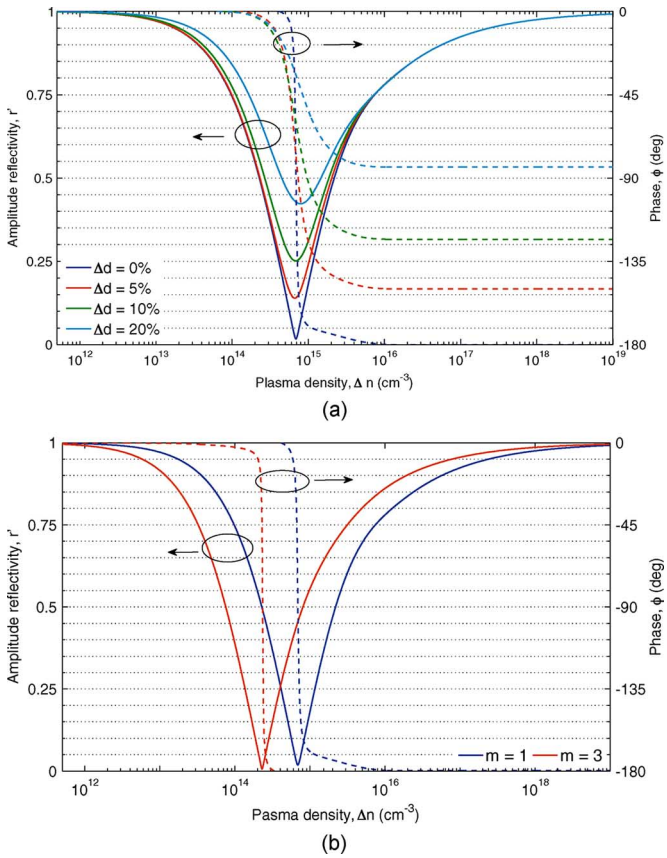

Fig. 6. Simulated transmission line properties for the reflection-type piFZPA, highlighting the required selection of the substrate thickness; (a) illustrates the loss in *contrast* for small deviations in substrate thickness, d, and (b) illustrates the change in required plasma density, Δn, for a change in the resonant matched substrate thickness.

However, in practice this will only be the case for high lifetime wafers.

V. piFZPA Demonstration

The following describes preliminary proof-of-principle experiments obtained with a tx-piFZPA, at 94 GHz, utilizing a commercially available visible data projector. The piFZPA featured a transmission-type configuration due to its simplicity and lower tolerances on the substrate thickness, as outlined above.

The transmission-type piFZPA configuration utilized a folded feed arrangement in order to reduce blockage effects of both the mm-wave beam and the projected zone mask. The folded feed arrangement utilized a dichroic beam diplexer comprised of an optically transparent mm-wave reflector composed of a thin indium tin oxide (ITO) coated polyester film, which provided approximately 60% reflectivity at 94 GHz and >80% (visible) optical transparency. A standard, commercially available data projector was used as a broadband visible light source and optical spatial light modulator; the chosen SLM was a 6,000 ANSI lumens XGA Sanyo projector, which provided uniform illumination across the semiconductor substrate at visible wavelengths. The receive feedhorn was a standard W-band WR10 corrugated horn with 20 dBi gain, which enabled reasonable zone plate designs (number of zones and edge taper).

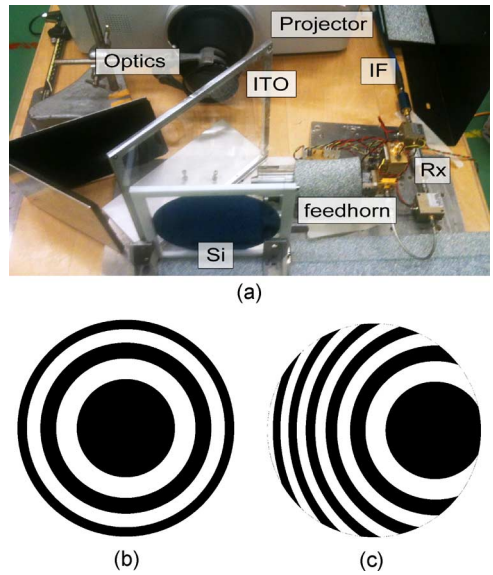

Fig. 7. (a) Photograph of the transmission-type piFZPA configured in receive mode. (b) Example projected zone plate mask for beam forming on-axis; and (c) example projected zone plate mask for off-axis beam forming at 10° from boresight.

Characterization of the piFZPA far-field antenna pattern was measured using a heterodyne receiver with a detector diode and a digital volt meter in order to measure the peak IF power. The test transmitter consisted of a Gunn oscillator and a standard WR10 20 dBi corrugated feedhorn, which was placed in the far-field of the piFZPA (>5 m).

The chosen semiconductor substrate was a processed [7] high-resistivity silicon wafer with an average resistivity of $\rho \approx 10,000\ \Omega\mathrm{cm}$, a minority effective lifetime of approximately $\tau_{\mathrm{eff}} \approx 1500\ \mu\mathrm{s}$, and a wafer thickness of approximately 600 μm. The silicon wafer was held upright with the aid of a bespoke HDPE frame.

The folded feed was then implemented via the ITO sheet which was angled 45° relative to the W-band feedhorn and the silicon wafer. The required zone plate masks were then projected using standard optics through the ITO sheet and onto the surface of the silicon wafer, resulting in a zone plate plasma within the substrate. Dynamic reconfiguration of the piFZPA was then controlled via suitable changes to the optically projected zone plate mask, i.e. changing the mask which is projected onto the silicon surface. Fig. 7(a) displays a photograph of the transmission-type piFZPA configured in receive mode, and Fig. 7(b) and 7(c) display example projected masks for forming a directive beam on- and off-axis, respectively.

The required sequence of zone plate masks for performing a particular 1-D or 2-D scan were generated in Matlab, and then loaded into bespoke software which controlled the display of each mask and syncing of measuring equipment; the custom software dynamically looped through each mask in the sequence and displayed each corresponding mask on the silicon wafer via the projector. Each mask (or pointing direction) consisted of a single JPEG image of approximately 100 kB file size with 1024 x 768 resolution, set by the native resolution of the data projector. The large file size used for these initial experiments limited the refresh rate of the piFZPA to less than 20 beams per

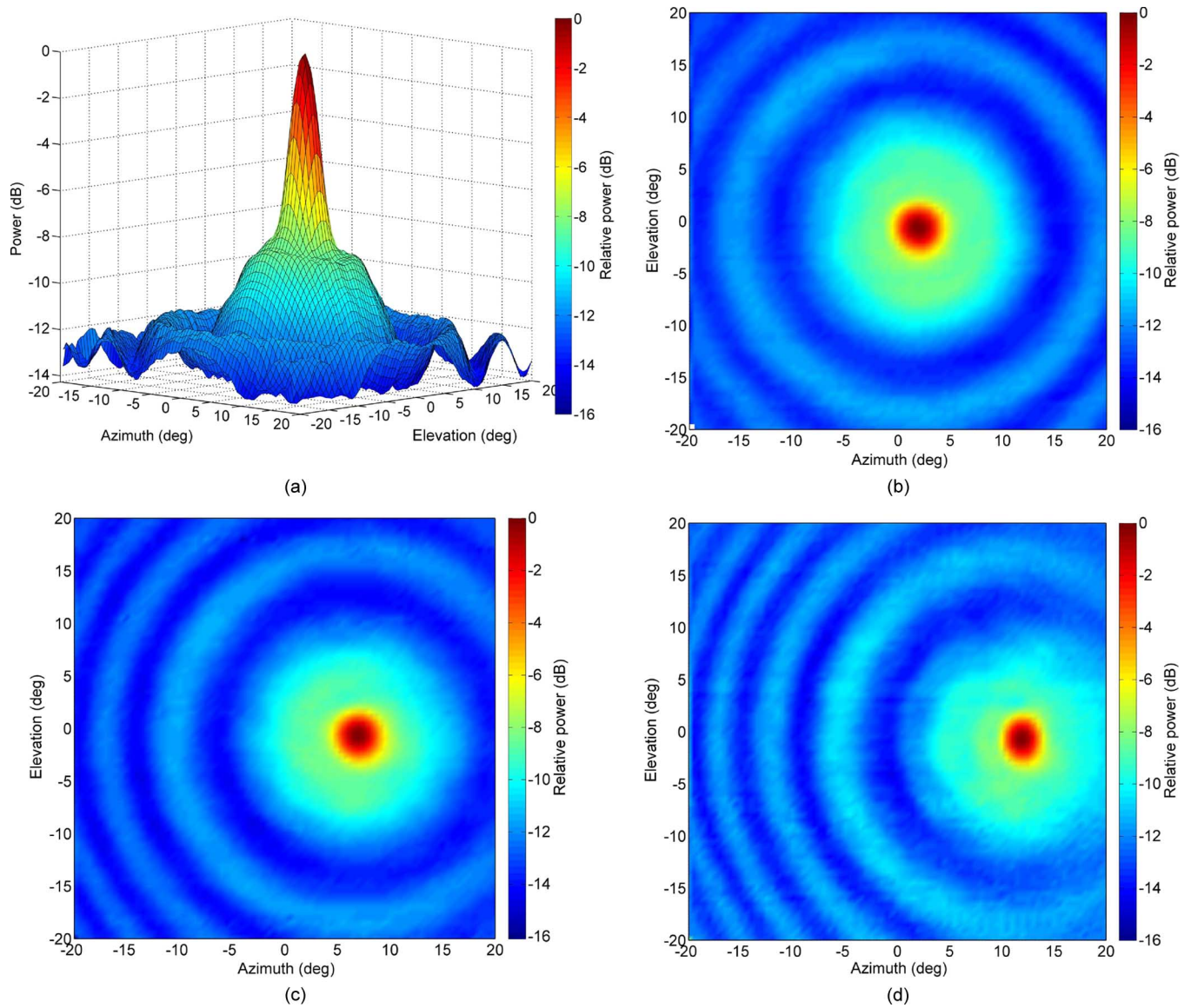

Fig. 8. Measured 2-D antenna pattern for an F/1.6, 100 mm diameter piFZPA with the transmitter fixed and located approximately at: (a), (b) boresight—$(\theta, \varphi) = (0^\circ, 0^\circ)$; (c) 5° from boresight—$(\theta, \varphi) = (+5^\circ, 0^\circ)$; and (d) 10° from boresight—$(\theta, \varphi) = (+10^\circ, 0^\circ)$.

second, although this could be easily increased with minor modification to the software. Nevertheless, the current configuration, based on the standard video projector, would have an upper beam rate limit of approximately 100 beams per second, which is set by refresh rates of commercial data projectors. However, piFZPAs do not require the full bit depth and color space commonly preconfigured for standard video displays, and thus their is considerable potential to achieve much higher rates.

The far-field response of the tx-piFZPA was measured by optically scanning the zone plate plasma over a pre-defined 2-D field-of-view that spanned the mainlobe of the piFZPA while the transmitter horn remained fixed. The piFZPA design featured a 160 mm focal length with a 100 mm effective aperture (see Fig. 7(b)). The irradiation density of the illuminated regions were measured to be approximately 70 $\mathrm{mW/cm^2}$ (measured using a thermopile), which yielded [9] a plasma density of approximately $\Delta n \approx 1.4 \times 10^{15}\ \mathrm{cm^{-3}}$.

The measured far-field pattern was performed over a 2-D area surrounding the fixed transmitter, spanning $\pm 20^\circ$ in both azimuth and elevation in 0.5° steps in both planes. This particular scan sequence required 6,561 zone masks, which resulted in a total sequence memory of 641 MB using the current JPEG image scheme.

Fig. 8(a) and 8(b) display the measured 2-D antenna pattern of the tx-piFZPA with the transmitter located (approximately) on-axis. The piFZPA is shown to feature an excellently formed, highly symmetrical beam with a distinct highly directive mainlobe and low level sidelobes. The moderate number of zones (see Fig. 7(b)) resulted in a reasonable sidelobe suppression with a peak sidelobe level of approx. -8.5 dB, formed symmetrically around the mainlobe. The half-power beamwidth was measured as 3.31°, and 3.36° in the H- and E- plane respectively, larger than the diffraction limit ($\approx 2^\circ$). The non-diffraction limited performance, in this case, was a result of free-carrier diffusion

effects, caused by the long free-carrier lifetime of the wafer, and as a result of the poor edge taper (approx. -15 dB) of the zone plate design, which was restricted by the WR10 horn used.

For the measured beamwidth angles, the directivity of the tx-piFZPA can be calculated to yield 35.1 dBi. The gain of the piFZPA was measured using the gain transfer method against a standard 20 dBi corrugated horn, and was found to be approximately 18 dBi, including a 4 dB loss resulting from the unmatched substrate thickness ($d = 600\ \mu\mathrm{m}$); such a loss is in agreement to that predicted by Fig. 3(a). Excluding this loss, the gain of the piFZPA was 22 dBi, implying a 4.8% effective radiation efficiency, which is lower than the maximum theoretical efficiency of 10% due to: (1) the limited output power available from the projector, i.e. $\Delta n < 10^{16}\ \mathrm{cm}^{-3}$ (see Fig. 3(a)), (2) degraded performance resulting from diffusion effects induced by the high free-carrier lifetime substrate, and (3) the poor edge taper of the zone plate design.

Fig. 8(c) and 8(d) display the measured 2-D far-field response of the tx-piFZPA with the transmitter located at $(\theta, \varphi) = (+5^\circ, 0^\circ)$ and $(\theta, \varphi) = (+10^\circ, 0^\circ)$, everything else remaining the same, where Fig. 7(c) demonstrates an example zone plate mask which forms a beam 10° off-axis in the azimuth plane.

The Off-axis measurements were repeated at a range of angles up to 45° from boresight for several F/D combinations. The peak power of the far-field response has been observed to drop by up to 7 dB at 30° deflection, increasing to 12 dB at 45° deflection from boresight. Astigmatism was also observed in these scans, as observed in Fig. 8(d), which is believed to have resulted from the non-optimal zone plate mask designs [9]. The measured drop in the off-axis peak power is in line with initial data presented by Webb *et al.*, which were obtained using the bespoke NIR LED architecture mentioned previously [4].

VI. Discussion and Conclusion

The photo-injected Fresnel zone plate antenna (piFZPA) proves to be a promising alternative to dynamic beam forming, and non-mechanical steering, and is suitable for a wide range of applications.

piFZPAs have been shown to be categorized as either transmission- or reflection-type. Transmission-type piFZPAs permit a single mode of operation: referred to as a blocking scheme; while the reflection-type permits two modes of operation: a blocking scheme, and a phase-reversal scheme. Both blocking schemes feature a maximum 10% radiation efficiency, or a 10 dB loss, while the phase-reversal scheme features a maximum radiation efficiency of 40%, or a 4 dB loss, comparable to alternative techniques such as Rotman lenses. For example, a 150 mm diameter piFZPA, at 94 GHz, would yield a directive gain of approximately 44 dBi, which would result in a maximum gain of 34 dBi for the blocking piFZPA configurations, and 40 dBi for the phase-reversal piFZPA configuration. While both configurations feature less than 100% radiation efficiency, both schemes enable rapid control of a highly directive, diffraction-limited beam over a 2-D area, using a simple, moderately low-cost, and highly flexible architecture. piFZPAs are thus an attractive option for a range of applications which are more typically limited by suitable beam steering technologies, rather than signal-to-noise, e.g. imaging, surveillance, remote sensing.

Each piFZPA configuration features an etalon with a distinct finesse, which results in differing sensitivities to changes in the substrate complex refractive index and thickness. Both effects lead to different free-carrier plasma density (and optical illumination) requirements and varying tolerances to the substrate thickness.

The required free-carrier plasma density, or optical illumination requirement, is shown to play a pivotal role in the performance of piFZPAs, whilst also determining the overall beam rates. Transmission-type piFZPAs require larger free-carrier plasma densities in order to achieve maximum radiation efficiency, and thus gain; however, the required optical irradiance levels, which scale with increasing required beam rates, often become impractical. Nevertheless, lower carrier density, non-metallic (absorbing) zones have been shown to enable significant reductions in the required irradiance level, with modest degradation to piFZPA performance, with a directive beam having been shown to form for optical excitations which generate as little as 2–3 dB of attenuation in alternating blocking zones. Nevertheless, attenuations exceeding 6–10 dB are shown to create directive beams which are near the theoretical maximum of the device, with minimal loss in gain and radiation efficiency, whilst maintaining near diffraction-limited angular resolution.

Alternatively, a blocking reflection-type piFZPA is shown to enable full 10% radiation efficiency with an order of magnitude less free-carrier density requirement, and thus permitting increased beam rates that feature practical irradiance levels.

Preliminary data for a 100 mm diameter transmission-type piFZPA based on standard display technologies is given. The F/1.6 tx-piFZPA device featured a highly symmetrical directive mainlobe, which was designed and characterized at 94 GHz. The performance of the piFZPA was below optimal due to the limited output power of the projector and the non-optimal amplitude taper provided by the feedhorns used. The resulting degradation is in agreement with that predicted by the theory discussed.

Given that the piFZPA can be fully optimized for a given application, with control over the required optical irradiance, refresh rate, efficiency, directivity, mm-wave frequency, and optical excitation wavelength, the piFZPA proves to be a promising low-cost and compact alternative for non-mechanical beam forming and 2-D (or 3-D) beam steering applications.

Acknowledgment

The authors would like to thank Dr. A. Holt and R. Sondena of the Institute for Energy Technology (IFE), Kjeller, Norway, for processing the silicon wafers used in Section V.

References

[1] C. H. Lee, P. S. Mak, and A. P. DeFonzo, "Optical control of millimeter-wave propagation in dielectric waveguides," *IEEE J. Quantum Electron.*, vol. QE-16, no. 3, pp. 277–288, Mar. 1980.

[2] V. A. Manasson, L. S. Sadovnik, V. A. Yepishin, and D. Marker, "An optically controlled MMW beam-steering antenna based on a novel architecture," *IEEE Trans. Microw. Theory Tech.*, vol. 45, no. 8, pp. 1497–1500, August 1997.

[3] G. W. Webb and L. H. Pinck, "Light-controlled MMW beam scanner," in *Proc. SMBO Int. Microwave Conf. Brazil*, 1993, pp. 417–422.
[4] G. W. Webb, S. C. Rose, M. S. Sanchez, and J. M. Osterwalder, "Experiments on an optically controlled 2-D scanning antenna," presented at the Antenna Applications Symp., Allerton Park, Monticello, IL, Sep. 16–18, 1998.
[5] G. W. Webb, W. Vernon, M. S. Sanchez, S. C. Rose, and S. Angello, "Optically controlled millimeter wave antenna," in *Proc. Int. Topical Meeting on Microwave Photonics*, 1999, pp. 275–278.
[6] G. W. Webb, S. Angello, W. Vernon, M. S. Sanchez, and S. C. Rose, "Novel photonically controlled antenna for MMW communication," in *Proc. Int. Topical Meeting on Microwave Photonics*, Sep. 2000, pp. 97–100.
[7] T. F. Gallacher, R. Sondena, D. A. Robertson, and G. M. Smith, "Optical modulation of millimeter-wave beams using a semiconductor substrate," *IEEE Trans. Microw. Theory Tech.*, vol. 60, no. 7, pp. 2301–2309, 2012.
[8] H. Hristov, *Fresnel Zones in Wireless Links, Zone Plate Lenses and Antennas*. Norwood, MA: Artech House Inc., 2000.
[9] T. F. Gallacher, "Optoelectronic Modulation of mm-wave beams using a photo-injected semiconductor substrate," Ph.D. dissertation, University of St Andrews, Scotland, U.K., Mar. 2012.
[10] B. J. Reits, "Adjustable microwave antenna," U.S. patent no. 5736966, Apr. 1998.
[11] G. W. Webb and S. G. Angello, "Plasma controlled antenna," U.S. patent no. 6621459, Sep. 2003.

Tom F. Gallacher (S'09) was born in Glasgow, Scotland, in 1985. He received the M.Phys.(Hons.) and the Ph.D. degree in physics from the University of St Andrews, Scotland, U.K., in 2008 and 2012, respectively.

His research interests include sub-millimeter and millimeter wave technologies and their interaction, and use thereof, with optically excited semiconductor materials. His Ph.D. research has been focused on optically excited semiconductor substrates for dynamic reconfigurable (sub) mm-wave spatial modulators, with focus on photo-injected Fresnel zone plate (piFZPA) devices. His past research has included: millimeter wave measurement techniques, FMCW radar, FMCW Doppler radar, and antenna measurements at millimeter wave and sub-millimeter wave frequencies.

Dr. Gallacher was a student member of the Institute of Physics 2003 to 2008, and a student member of the Antenna and Propagation Society in 2009–2010.

Duncan A. Robertson (S'91–M'94) was born in Aberfeldy, U.K., in 1969. He received the B.Sc.(Hons) degree in physics and electronic and the Ph.D. degree in millimetre wave physics from the University of St Andrews, St Andrews, Fife, U.K., in 1991 and 1994 respectively.

From 1994 to 1999, he was a Research Fellow with the Millimetre Wave Group, University of St Andrews, under contract to DERA Malvern, working on battlefield millimetre wave systems. Between 1999 and 2000, he was a Principal Microwave Engineer with Racal-MESL, Edinburgh, U.K., working on high power radar duplexers. From 2000 to 2004, he worked in the Photonics Innovation Centre, University of St Andrews, commercializing millimetre wave technology. Since 2004, he has been a Research Fellow with the Millimetre Wave and EPR Group, University of St Andrews. His research interests include millimetre wave radar, radiometry, imaging, electron paramagnetic resonance instrumentation, materials characterisation (ferrites, dielectrics and absorbers) and antennas (corrugated horns, quasi-optics and non-mechanical beam steering).

Dr. Robertson is a Chartered Physicist, a member of the Institute of Physics, a member of the Institute of Engineering and Technology and a member of SPIE.

Graham M. Smith was born in Karlsuhe, West Germany, in 1963. He received the B.Sc. degree in theoretical physics from York University, and the M.Sc. degree in lasers and optoelectronics and the Ph.D. degree in millimeter-wave physics from the University of St Andrews.

His research interests mainly involve mm-wave instrumentation system and component design and mm-wave electron paramagnetic resonance spectroscopy. He currently leads the MM-Wave and EPR group at the University of St Andrews.

Dr. Smith he won the 2011 Silver Medal for Instrumentation from the International EPR Society for his work on high power pulsed EPR.